



Photometric and Spectroscopic Study of Two Low Mass Ratio Contact Binary Systems: CRTS J225828.7-121122 and CRTSJ030053.5+230139

Surjit S. Wadhwa¹ , Jelena Petrović², Nick F. H. Tohill¹, Ain Y. De Horta¹, Miroslav D. Filipović¹, and Gojko Djurašević²
¹School of Science, Western Sydney University, Locked Bag 1797, Penrith, NSW 2751, Australia; 19899347@student.westernsydney.edu.au
²Astronomical Observatory, Volgina 7, 11060 Belgrade, Serbia

Received 2023 July 21; revised 2023 August 17; accepted 2023 August 24; published 2023 October 4

Abstract

The study reports photometric and spectroscopic observations of two recently recognized contact binary systems. Both systems show total eclipses and analysis of the light curves indicates both have very low mass ratios of less than 0.3. We derive absolute parameters from color and distance based calibrations and show that, although both have low mass ratios, they are likely to be in a stable orbit and unlikely to merge. In other respects, both systems have characteristics similar to other contact binaries with the secondary larger and brighter than their main sequence counterparts and we also find that the secondary is considerably denser than the primary in both systems.

Key words: (stars:) binaries: eclipsing – stars: mass-loss – techniques: photometric

1. Introduction

As the number of cataloged contact binaries grows with each new sky survey, opportunities for their study have also been enhanced. In particular, interest in low mass ratio contact binaries is intense since the recognition that V1309 Sco (=Nova Sco 2008) was in fact a red nova resulting from the merger of contact binary components (Tylenda et al. 2011). Although a large number of low mass ratio contact binaries have been identified (Gazeas et al. 2021; Christopoulou et al. 2022; Li et al. 2022; Liu et al. 2023) only a handful meet the theoretical criteria for orbital stability (Wadhwa et al. 2022a, 2023a). Wadhwa et al. (2022b) recently outlined an efficient method for identifying low mass ratio contact binaries from survey based light curves without formal analysis. We use the methods described in Wadhwa et al. (2022b) to select two potential low mass ratio contact binaries for follow up ground based observations.

CRTS J225828.7-121122 (C2258) ($\alpha_{2000.0} = 225828.73$, $\delta_{2000.0} = -121122.3$) (=ASAS J225829-1211.3, ASASSN-V J225828.64-121121.9) was recorded as a contact binary system by the All Sky Automated Survey (ASAS) (Pojmanski 2002) with maximum V band magnitude of 13.37 and period of 0.25208 day. CRTS J030053.5+230139 (C0300) ($\alpha_{2000.0} = 030053.60$, $\delta_{2000.0} = 230139.2$) (=ASAS J030054+2301.7, ASASSN-V J030053.58+230138.7) was also identified by ASAS with brightest V magnitude of 13.46 and period of 0.363298 day. Based on the relationships described by Wadhwa et al. (2022b), we estimated that both systems are likely to have low mass ratio and as such carried out follow up ground based observations and analysis. In addition, both systems were also observed by the Transiting Exoplanet Survey

Satellite (TESS) mission. TESS photometry recorded the amplitude of 0.50 mag for C2258 and 0.42 mag for C0300.

2. Observations

2.1. Photometric Observations

C2258 was observed over 3 days in 2022 August with the Las Cumbres Observatory (LCO) network of 0.4 m telescopes using an SBIG STL-6303 CCD camera and Bessel V and B filters. In total, 217 images were acquired in V band and 40 additional images were acquired in B band during total eclipses to document the $B - V$ value. The AstroImageJ (Collins et al. 2017) package was utilized to perform differential photometry. TYC 5816-873-1 was the comparison star and 2MASS 22581807-1207490 was the check star. Comparison and check star magnitudes were taken from the AAVSO Photometric All-Sky Survey (Henden et al. 2015) calibrations. We find the brightest magnitude to be slightly fainter than survey data at 13.47 mag with no significant difference in the two maxima. The primary eclipse has a magnitude of 13.99 indicating an amplitude of 0.52 mag while the secondary eclipse is slightly brighter at 13.94 mag. Both eclipses have a total duration of approximately 36 minutes. The mean B band magnitudes during the primary and secondary eclipses were 14.72 and 14.66 respectively, yielding a $B - V$ value of 0.72 for the system. Based on the single observed minimum and available survey based V band photometry, we revise the orbital elements as follows

$$\begin{aligned} \text{HJD}_{\min} &= 2459821.71100(\pm 0.00021) \\ &+ 0.2520799(\pm 0.000050)E. \end{aligned}$$

C0300 was similarly observed with the LCO network of 0.4 m telescopes over four nights in 2022 November. In total,

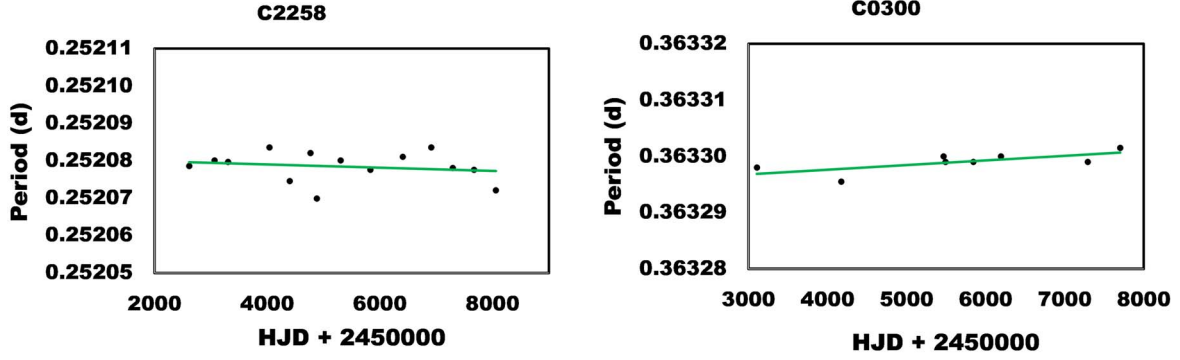


Figure 1. Period variation trend for C2258 (left) and C0300 (right). The green line represents the line of best fit.

268 images were acquired in V band and an additional 44 images were acquired in the B band to document the $B - V$ value. As for C2258, differential photometry was performed with the AstroImageJ package using 2MASS 03003069 +2259527 as the comparison star and 2MASS 03004569 +2256105 as the check star. Similar to C2258, both maxima are of similar magnitude at 13.51. Both eclipses are total with the primary eclipse slightly fainter at 14.02 mag, indicating an amplitude of 0.51 mag, and the secondary eclipse marginally brighter at 14.00 mag. Eclipse duration is similar to C2258 at approximately 32 minutes. The B band magnitudes at primary eclipse (14.8) and secondary eclipse (14.78) yield a $B - V$ value of 0.78 mag. Based on our single observed minimum and available survey based V band photometry, we revise the orbital elements as follows

$$\begin{aligned} \text{HJD}_{\min} &= 2459912.370060(\pm 0.000577) \\ &+ 0.36329667(\pm 0.000005)E. \end{aligned}$$

We note that the observed amplitude of C2258 is very similar to the TESS amplitude, differing by 0.02 mag, however the observed amplitude for C0300 is almost 0.1 mag greater compared to the TESS photometry. The discrepancy is likely due to blending of the TESS images from nearby fainter stars. TESS images are collected using four small aperture wide-field cameras with very wide point-spread function of approximately $1'$ (Sullivan et al. 2015), significantly increasing the chance of potential blending. A much more dramatic example of blending induced reduction in amplitude of a totally eclipsing contact binary, leading to an erroneous light curve solution, was described by Wadhwa et al. (2023b). That system was reported to have an extremely low mass ratio based on SuperWASP (Pollacco et al. 2006) photometry, with a resolution of approximately $1'$. The system was in fact a stable high mass ratio system with significantly higher amplitude. The difference in amplitude is reflected in the light curve solutions (see below), however we believe the ground based observations in this case yield more accurate results.

Assessment of period variation, especially when small, requires high cadence observations over a long term (many decades). Given the lack of suitable historical observations (most survey data have a cadence of many days between single observations), no meaningful Observed – Computed ($O - C$) analysis could be performed for either system. Instead, we use the technique employing periodic orthogonal polynomials and an analysis of variance statistic (a quality of fit marker) to fit multiple overlapping subsets, each of approximately 100–150 observations, of V , g' and R band data from various surveys including ASAS, All Sky Automated Survey for SuperNovae (ASAS-SN) (Shappee et al. 2014; Jayasinghe et al. 2020), Catalina Surveys (Drake et al. 2017) and Zwicky Transient Facility (ZTF) (Masci et al. 2019) for each system to estimate any significant period variations. The SuperWASP (Pollacco et al. 2006) data for C0300 proved unsuitable due to significant scatter and high reported errors. This is not surprising given the brightness of C0300 is near the faint magnitude limit for the survey. The methodology is described in detail by Schwarzenberg-Czerny (1996) and was utilized by Tylanda et al. (2011) to demonstrate the exponential decay in the period of V1309 Sco, the only confirmed contact binary merger system. For C2258, there is a slight linear decrease in period of -1.58×10^{-7} days per year while for C0300 there is a linear increase in period of 3.03×10^{-7} days per year. The period trends are illustrated in Figure 1.

2.2. Effective Temperature and Spectroscopic Observations

Analysis of contact binary light curves can be successfully carried out where the light curve demonstrates total eclipses (Terrell & Wilson 2005). During analysis, the primary component temperature (T_1) is usually fixed and nonadjustable. The shape of contact binary light curves is almost completely dependent on the Roche geometry and parameters such as the inclination (i), mass ratio (q) and Roche equipotential (=degree of contact- f) (Rucinski 1993, 2001; Wadhwa et al. 2022b). Although the light curve shape places a tight constraint on the component

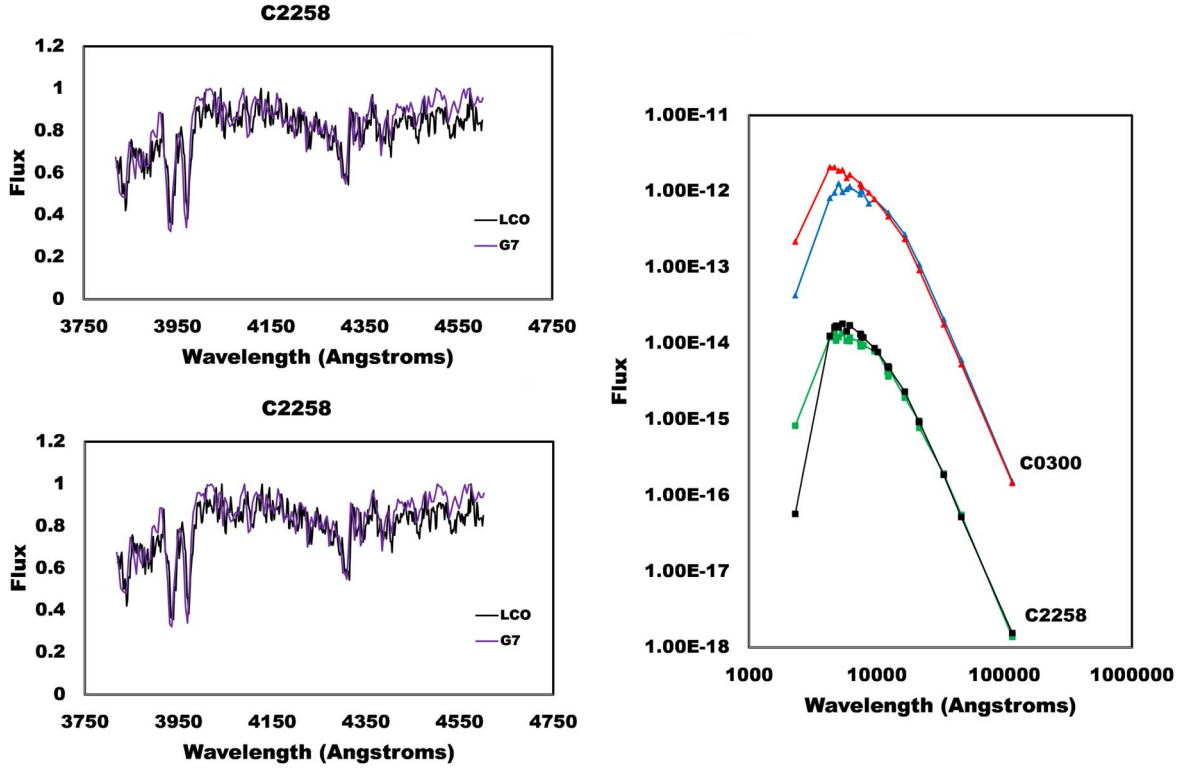


Figure 2. Left panel: LCO and LAMOST with standard library spectra for C2258 and C0300. Right panel: Observed (green and blue) and modeled (black and red) SEDs for C0300 and C2258. The vertical flux is in $\text{erg cm}^{-2} \text{s}^{-1} \text{\AA}^{-1}$ and has been shifted vertically by $\times 10^2$ for C0300 for clarity.

temperature (T_2/T_1) ratio, the absolute value of T_1 has little influence on the determined geometric elements (Rucinski 1993, 2001). Previous color based estimates for T_1 have been used, however these have proven to be troublesome given the wide variation in cataloged values based on different colors and calibrations. In the case of C2258, the VizieR catalog service has a range of 5388–5923 K for the effective temperature of the system and for C0300 the range is even wider at 5076–6001 K. Although no standard calibration has been adopted, many investigators are moving to low resolution spectral observation and spectral class calibration as a means of assigning the effective temperature (see e.g., Zhou et al. 2018; Chang et al. 2022; Guo et al. 2022). We acquired a low resolution spectrum of C2258 using the FLOYDS spectrographs attached to the 2 meter telescopes of the LCO network. The spectrum of C2258 was visually matched to a library of spectra of main sequence stars (Jacoby et al. 1984; Pickles 1998) to determine its spectral class is G7. C0300 was observed by the Large Sky Area Multi-Object Fiber Spectroscopic Telescope (LAMOST) with a reported spectral class of G1 (Luo et al. 2018). The acquired and library spectra of C2258 and the LAMOST and library spectra of C0300 are shown in the left panel of Figure 2. We used the 2022 April update of the Pecaut & Mamajek (2013) calibration tables for main sequence stars to determine the temperature of the

primary components based on the determined spectral class. The assigned temperature for C2258 was 5550 K and that for C0300 was 5860 K. The values are within the wide cataloged ranges for both systems.

To further confirm the utility of spectral classification based estimation of the effective temperature, we compared the values against a collective photometric approach which collates the photometric data from various pass-bands to construct a single Spectral Energy Distribution (SED) (Bayo et al. 2008). The SED is then fitted against synthetic theoretical spectra using χ^2 minimization along with Kurucz atmospheric models (Bayo et al. 2008) to determine the effective temperature. The SED estimated effective temperature for C2258 was 5500 and it was 5750 K for C0300. Given the good agreement between photometric and spectral classification in estimating the effective temperature, we consider the use of spectral classification as a valid approach to assign the temperature of the primary component and we have followed this in this study. The SED and fitted model are depicted in the right panel of Figure 2.

3. Light Curve Solutions and Physical Parameters

As noted above, both systems exhibit total eclipses and thus are likely to yield accurate light curve solutions. We used the 2013

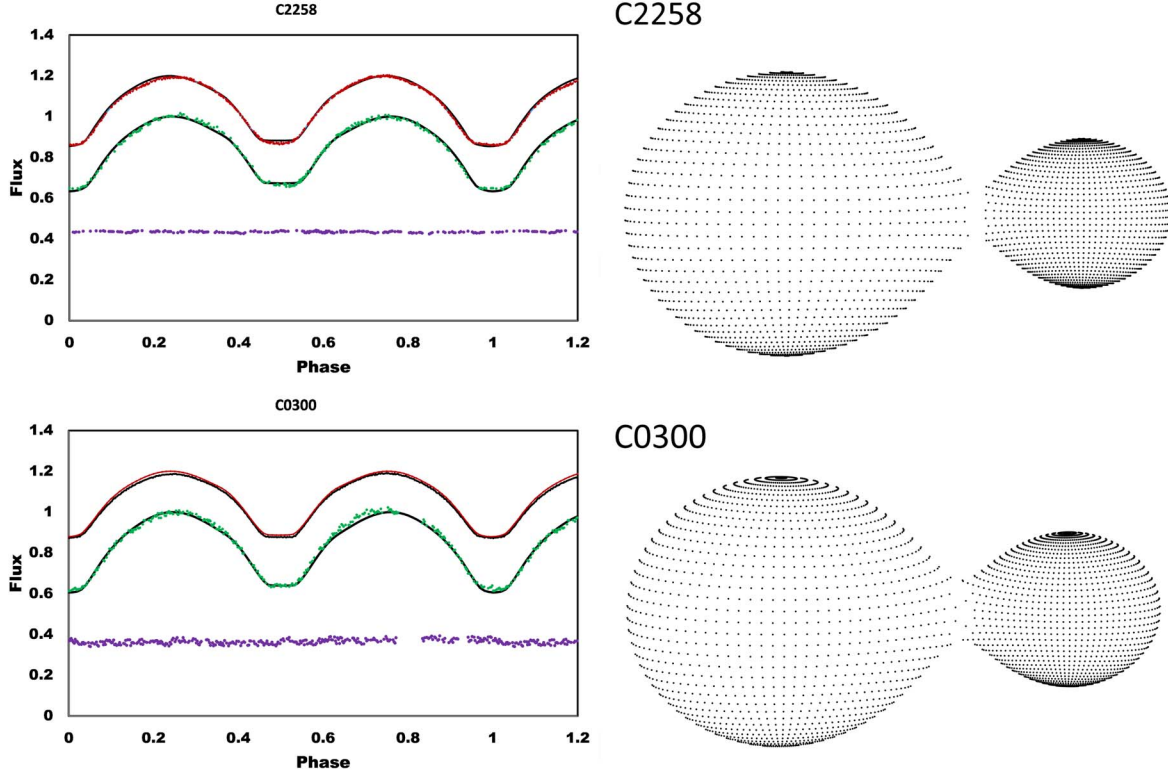


Figure 3. Observed (green), TESS (red), fitted (black) and check (purple) light curves for C2258 and C0300 along with corresponding 3D representations. The TESS curves have been shifted vertically for clarity.

version of the Wilson-Devinney code to analyze the V band photometry data. We employed the tried and tested q search/grid method to obtain the mass ratio and complete light curve solution for each system. As there is no appreciable difference in the two maxima for either system, only unspotted solutions were modeled. As is usual for low temperature systems, the bolometric albedos and gravity darkening coefficients were fixed at ($A_1 = A_2 = 0.5$) and ($g_1 = g_2 = 0.32$) respectively, and simple reflection treatment applied. We interpolated limb darkening coefficients from van Hamme (1993) (2019 update). The filter used by the TESS mission is quite broad, ranging from 600 to 1000 nm centered near the Ic band (786.5 nm). We applied the limb darkening coefficients centered on the Ic band for analyzing the TESS photometry. Fitted and observed light curves and three-dimensional (3D) representations of the contact binaries are displayed in Figure 3. The light curve solutions are summarized in Table 1.

The light curve solution provides the mass ratio and fractional radii of the components among other geometric parameters. To fully determine the absolute physical parameters, one needs to estimate the mass of the primary (M_1). There is no direct method, however secondary calibrations have proven effective. For this study, we adopt the mean of an infrared color ($J - H$) calibration and an absolute magnitude

calibration based on distance. We obtained the ($J - H$) color for both systems from the Two Micron All Sky Survey (2MASS) (Skrutskie et al. 2006) and we referenced the calibration tables of Pecaut & Mamajek (2013) (2022 April update) for low mass ($0.6M_\odot < M < 1.4M_\odot$) stars to interpolate the mass of the primary component.

As the mass ratios are well below 1, the apparent magnitude of the primary component is equal to the apparent magnitude at the secondary eclipse. We can use this along with the distance to estimate the absolute magnitude of the primary component. The apparent magnitude of the primary component was first corrected for reddening and distance as follows: Reddening at infinity $E(B - V)_\infty$ was determined from Schlafly & Finkbeiner (2011) dust maps. This value was then distance scaled to $E(B - V)_d$ based on the Gaia Data Release 3 (DR3) (Anders et al. 2022) distance for each system as per the equation (Bilir et al. 2008)

$$E(B - V)_d = E(B - V)_\infty \left[1 - \exp\left(-\frac{|d \sin b|}{h}\right) \right]. \quad (1)$$

In the equation, d is the Gaia distance in parsecs, b is the galactic latitude and h is the galactic scale height, adopted as $h = 125$ pc (Bilir et al. 2008). The $E(B - V)_d$ for C2258 and

Table 1
Light Curve Solution and Physical Parameters of C2258 and C0300

Parameter	C2258	C2258 (TESS)	C0300	C0300 (TESS)
T_1 (K) (Fixed)	5550	5500	5860	5860
T_2 (K)	5536 ± 15	5540 ± 10	5846 ± 16	5956 ± 10
Inclination ($^\circ$)	88.3 ± 1.7	87.4 ± 0.6	83.2 ± 0.7	80.4 ± 0.1
Fill-out (%)	20 ± 3	23 ± 3	28 ± 4	15 ± 4
r_1 (mean)	0.516	0.518	0.505	0.517
r_2 (mean)	0.273	0.275	0.292	0.269
q (M_2/M_1)	0.240 ± 0.005	0.240 ± 0.010	0.287 ± 0.003	0.233 ± 0.002
A/R_\odot	1.71 ± 0.01		2.28 ± 0.02	
M_1/M_\odot	0.85 ± 0.02		0.94 ± 0.02	
M_2/M_\odot	0.21 ± 0.01		0.27 ± 0.01	
R_1/R_\odot	0.88 ± 0.02		1.15 ± 0.02	
R_2/R_\odot	0.47 ± 0.01		0.67 ± 0.02	
M_{V1}	5.92 ± 0.08		4.83 ± 0.06	
$\Delta\rho$	-1.20		-0.43	

C0300 were determined as 0.031 and 0.183 respectively, and the distance corrected extinctions were 0.1 and 0.57 mag respectively. The absolute magnitude of the systems was then determined using the standard distance modulus. We again referenced the updated Pecaut & Mamajek (2013) tables for low mass stars to interpolate the mass of the primary based on absolute magnitude. We adopted the mean of the infrared and absolute magnitude calibration for the mass of the primary for subsequent calculations. As the distance based determinations yielded the highest potential errors, these were adopted and propagated.

Having determined M_1 (and M_2 based on the mass ratio q), we can take advantage of Kepler's third law to estimate the current separation (A) between the components. Fractional radii of the components are provided in three orientations by the light curve solution, and the geometric mean of these ($r_{1,2}$) can be employed to determine the absolute component radii ($R_{1,2}$) as follows: $R_{1,2} = A(r_{1,2})$.

Utilizing the mean fractional radii, we can express the difference in component densities as follows

$$\Delta\rho = \frac{0.0189q}{r_2^3(1+q)P^2} - \frac{0.0189}{r_1^3(1+q)P^2}. \quad (2)$$

Some researchers argue that contact binary evolution may actually result in a change in component designation such that the current primary may have been the initial secondary while the current secondary could have been the initial primary that lost mass to the current primary. The end result of such a scenario is that the current secondary is rich in core like or heavier elements and the current primary rich in lighter elements. Researchers have argued that the densities of the components therefore must differ such that the secondary will always be denser than the primary and $\Delta\rho$ will always be less than zero which is confirmed in both cases (Kähler 2004). The physical parameters are summarized in Table 1.

A different approach to estimating absolute parameters is to use standard blackbody emissions based on the determined luminosity as described in Li et al. (2021). Following this approach with our determined values of the absolute magnitude of the primary, we derive M_1 , M_2 , R_1 and A as $0.74M_\odot$, $0.18M_\odot$, $0.71R_\odot$ and $1.63R_\odot$ for C2258 and $0.98M_\odot$, $0.28M_\odot$, $0.97R_\odot$ and $2.32R_\odot$ for C0300 respectively. We prefer to use estimates based on the geometric light curve solution principally due to the dependency of the blackbody estimates on the estimated effective temperature. As noted above, the cataloged effective temperatures of the two systems described vary by many hundreds of degrees. A change in the effective temperature of ± 200 K for C2258 leads to a range in M_1 from $0.67M_\odot$ to $0.8M_\odot$ and for C0300 from $0.94M_\odot$ to $1.03M_\odot$. As noted above, the absolute value of the effective temperature has no significant influence on the geometric light curve solution such that small variations in temperature will not significantly effect absolute parameter estimates determined using light curve solution elements. In addition to the dependency on the effective temperature, the blackbody based estimate requires multiple steps such as determination of luminosity then radius and then mass of the component. Each step requires error propagation potentially reducing the confidence in the estimated value. Lastly, methodology based on the geometric solution incorporates the distorted morphology of contact binary systems by utilizing the geometric mean of the fractional radii in different orientations as opposed to a spherical configuration for blackbody estimates. As noted by Wadhwa et al. (2022b), although the primary components of contact binary systems in general follow main sequence characteristics, their radii are usually somewhat larger, as reflected in this report.

At present, there is significant interest in orbital stability of contact binary systems. Wadhwa et al. (2021) recently defined simplified relationships between light curve geometric elements

and the mass of the primary with orbital instability. They showed that for low mass primaries the instability mass ratio (q_{inst}) is between

$$q_{\text{inst}} = 0.0772 M_1^2 - 0.3003 M_1 + 0.3237 (f = 0) \quad (3)$$

and

$$q_{\text{inst}} = 0.1269 M_1^2 - 0.4496 M_1 + 0.4403 (f = 1). \quad (4)$$

The equation represents the extremes of the instability mass ratio at marginal contact ($f=0$) and complete overcontact ($f=1$).

Based on the equations above, the instability mass ratio range for C2258 is 0.124-0.15 and that for C0300 is 0.11-0.13. The light curve solution indicates mass ratios well above the instability mass ratio range, suggesting that both systems are likely stable and not merger candidates.

4. Summary and Conclusion

Contact binaries represent ideal systems for the study of not only stellar evolutionary scenarios but also orbital dynamics. Orbital stability has received considerable attention recently (Wadhwa et al. 2021; Christopoulou et al. 2022; Liu et al. 2023) and it is clear from earlier works that contact binaries are likely to become unstable at low mass ratios (Arbutina 2007, 2009). Based on some simplified criteria (Wadhwa et al. 2022b), we selected two systems showing total eclipses on survey photometry (hence being suitable for light curve analysis) that also were likely to have a low mass ratio. Our results confirm that both systems indeed have low mass ratio at less than 0.3, however once we estimate the physical parameters, such as the mass of the primary, it is clear that both systems are not near the instability parameters and as such not potential merger candidates. The study does however confirm that recently published selection and analysis relationships can be easily implemented to selectively observe low mass ratio contact binary systems.

Acknowledgments

This research has made use of the VizieR catalog access tool, CDS, Strasbourg, France (DOI: [10.26093/cds/vizier](https://doi.org/10.26093/cds/vizier)).

This research has made use of the SIMBAD database, operated at CDS, Strasbourg, France.

This work makes use of observations from the Las Cumbres Observatory global telescope network.

This publication makes use of VOSA, developed under the Spanish Virtual Observatory (<https://svo.cab.inta-csic.es>) project funded by MCIN/AEI/10.13039/501100011033/ through grant PID2020-112949GB-I00. VOSA has been partially updated by using funding from the European Union's Horizon

2020 Research and Innovation Programme, under grant Agreement No. 776403 (EXOPLANETS-A).

J.P. and G.D. gratefully acknowledge financial support of the Ministry of Education, Science and Technological Development of the Republic of Serbia through contract No. 451-03-9/2021-14/200002.

ORCID iDs

Surjit S. Wadhwa  <https://orcid.org/0000-0002-7011-7541>

References

- Anders, F., Khalatyan, A., Queiroz, A. B. A., et al. 2022, *A&A*, **658**, A91
- Arbutina, B. 2007, *MNRAS*, **377**, 1635
- Arbutina, B. 2009, *MNRAS*, **394**, 501
- Bayo, A., Rodrigo, C., Barrado Y Navascués, D., et al. 2008, *A&A*, **492**, 277
- Bilir, S., Ak, S., Karaali, S., et al. 2008, *MNRAS*, **384**, 1178
- Chang, L.-F., Zhu, L.-Y., Sarotsakulchai, T., & Soonthornthum, B. 2022, *PASJ*, **74**, 1421
- Christopoulou, P.-E., Lalounta, E., Papageorgiou, A., et al. 2022, *MNRAS*, **512**, 1244
- Collins, K. A., Kielkopf, J. F., Stassun, K. G., & Hessman, F. V. 2017, *AJ*, **153**, 77
- Drake, A. J., Djorgovski, S. G., Catelan, M., et al. 2017, *MNRAS*, **469**, 3688
- Gazeas, K. D., Loukaidou, G. A., Niarchos, P. G., et al. 2021, *MNRAS*, **502**, 2879
- Guo, D.-F., Li, K., Liu, F., et al. 2022, *MNRAS*, **517**, 1928
- Henden, A. A., Levine, S., Terrell, D., & Welch, D. L. 2015, AAS Meeting Abstracts, **225**, 336.16
- Jacoby, G. H., Hunter, D. A., & Christian, C. A. 1984, *ApJS*, **56**, 257
- Jayasinghe, T., Stanek, K. Z., Kochanek, C. S., et al. 2020, *MNRAS*, **491**, 13
- Kähler, H. 2004, *A&A*, **414**, 317
- Li, K., Gao, X., Liu, X.-Y., et al. 2022, *AJ*, **164**, 202
- Li, K., Xia, Q.-Q., Kim, C.-H., et al. 2021, *AJ*, **162**, 13
- Liu, X.-Y., Li, K., Michel, R., et al. 2023, *MNRAS*, **519**, 5760
- Luo, A. L., Zhao, Y. H., Zhao, G., et al. 2018, *yCat*, V/153
- Masci, F. J., Laher, R. R., Rusholme, B., et al. 2019, *PASP*, **131**, 018003
- Pecaut, M. J., & Mamajek, E. E. 2013, *ApJS*, **208**, 9
- Pickles, A. J. 1998, *PASP*, **110**, 863
- Pojmanski, G. 2002, *AcA*, **52**, 397
- Pollacco, D. L., Skillen, I., Collier Cameron, A., et al. 2006, *PASP*, **118**, 1407
- Rucinski, S. M. 1993, *PASP*, **105**, 1433
- Rucinski, S. M. 2001, *AJ*, **122**, 1007
- Schlafly, E. F., & Finkbeiner, D. P. 2011, *ApJ*, **737**, 103
- Schwarzenberg-Czerny, A. 1996, *ApJL*, **460**, L107
- Shappee, B. J., Prieto, J. L., Grupe, D., et al. 2014, *ApJ*, **788**, 48
- Skrutskie, M. F., Cutri, R. M., Stiening, R., et al. 2006, *AJ*, **131**, 1163
- Sullivan, P. W., Winn, J. N., Berta-Thompson, Z. K., et al. 2015, *ApJ*, **809**, 77
- Terrell, D., & Wilson, R. E. 2005, *Ap&SS*, **296**, 221
- Tylenda, R., Hajduk, M., Kamiński, T., et al. 2011, *A&A*, **528**, A114
- van Hamme, W. 1993, *AJ*, **106**, 2096
- Wadhwa, S. S., Arbutina, B., Tothill, N. F. H., et al. 2023a, *PASP*, **135**, 074202
- Wadhwa, S. S., De Horta, A., Filipović, M. D., et al. 2021, *MNRAS*, **501**, 229
- Wadhwa, S. S., De Horta, A., Filipović, M. D., et al. 2022a, *RAA*, **22**, 105009
- Wadhwa, S. S., De Horta, A. Y., Filipović, M. D., et al. 2022b, *JApA*, **43**, 94
- Wadhwa, S. S., DeHorta, A. Y., Filipović, M., & Tothill, N. F. H. 2023b, *AN*, **344**, e20220066
- Zhou, X., Qian, S., Boonruksar, S., et al. 2018, *PASJ*, **70**, 87